PERGAMON

International Journal of Solids and Structures 39 (2002) 1949–1965

INTERNATIONAL JOURNAL OF SOLIDS and STRUCTURES

www.elsevier.com/locate/ijsolstr

Dynamic stability analysis of composite plates including delaminations using a higher order theory and transformation matrix approach

Adrian G. Radu, Aditi Chattopadhyay *

Department of Mechanical and Aerospace Engineering, Arizona State University, P.O. Box 876106, Tempe, AZ 85287-6106, USA

Received 16 October 2000

Abstract

A refined higher order shear deformation theory is used to investigate the dynamic instability associated with composite plates with delamination that are subject to dynamic compressive loads. Both transverse shear and rotary inertia effects are taken into account. The theory is capable of modeling the independent displacement field above and below the delamination. All stress free boundary conditions at free surfaces as well as delamination interfaces are satisfied by this theory. The procedure is implemented using the finite element method. Delamination is modeled through the multi-point constraint approach using the transformation matrix technique. For validation purposes, the natural frequencies and the critical buckling loads are computed and compared with three-dimensional NASTRAN results and available experimental data. The effect of delamination on the critical buckling load and the first two instability regions is investigated for various loading conditions and plate thickness. As expected, the natural frequencies and the critical buckling load of the plates with delaminations decrease with increase in delamination length. Increase in delamination length also causes instability regions to be shifted to lower parametric resonance frequencies. The effect of edge delamination on the static and dynamic stability as well as of delamination growth is investigated.

Keywords: Composite plates; Higher order theory; Delamination; Dynamic stability

1. Introduction

Delamination between plies is one of the most common defect encountered in composite laminates. It can occur during manufacturing or it can be induced by various service loads and ultimately leads to structural failure. Therefore the behavior of structural members with delaminations has received considerable attention in recent years. In modeling delaminations, both, analytical (Simitses et al., 1985; Karadomateas and Schmueser, 1988) as well as numerical methods (Schivakumar and Whitcomb, 1985) have been used in studying the dynamic and buckling behavior of composite laminates. The higher order

* Corresponding author. Tel.: +1-480-965-9342; fax: +1-480-965-1384.
E-mail address: aditi@asu.edu (A. Chattopadhyay).

0020-7683/02/$ - see front matter
PII: S0020-7683(01)00168-8

theories (HOTs) which more accurately model transverse shear effects, have been shown to better predict the natural frequencies and critical buckling loads (Reddy, 1984; Reddy and Phan, 1985). A new refined HOT was developed by, Chattopadhyay and Gu (1994) to model delaminations in composite plates. The theory has been also applied on composite shells undergoing buckling and post-buckling (Gu and Chattopadhyay, 1996). This theory was validated with exact analytical solutions as well as experimental results (Gu and Chattopadhyay, 1998). Dynamic stability investigations of composite plates without delaminations have been performed using the classical laminate plate theory (CLPT) (Srinivasan and Chelepandi, 1986) and the first order shear deformation theory (FSDT) (Bert and Birman, 1987; Balamurugan et al., 1996). In a recent study, Chattopadhyay and Radu (2000) have also shown HOT to more accurately approximate the instability regions of composite plates without delaminations. The objective of the present work is to extend the application of the HOT to dynamic stability of composite plates with delaminations using a finite element approach. The HOT assumes a cubic distribution for the in-plane displacements through the thickness and satisfies the stress free boundary conditions at the top and bottom surfaces of the laminate and at the delamination interfaces. The delamination is modeled by imposing continuity conditions between the adjacent sub-laminates using the transformation matrix method (Cook et al., 1989). Composite plates with various thickness and delamination length and placement are analyzed. The developed finite element model is validated through natural frequencies, the critical buckling load results by comparison with available experimental data (Shen and Grady, 1992) and with those obtained from a three-dimensional (3D) NASTRAN analysis. The instability regions are determined for composite plates with and without delaminations and the results are presented for different delamination lengths and placement under various loading conditions.

2. Problem formulation

A composite plate with the coordinate plane (x, y) as the mid-plane and the z-axis along the thickness direction is considered. A through-the-width delamination divides the composite plate into four regions as shown in Fig. 1 where L and L_d represent plate and delamination length respectively. The delamination is considered symmetrically placed with respect to the edges of the plate, in the plate mid-plane. Quantities h_1 through h_4 denote the thickness of the upper, lower, left and right sub-laminates respectively. The upper and lower sub-laminates are denoted 1 and 2 respectively and the left and right sub-laminates are denoted 3

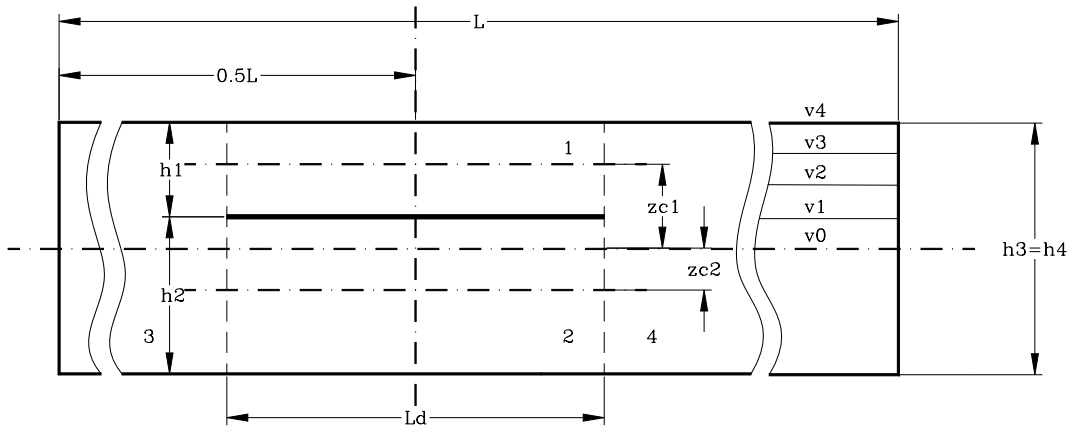

Fig. 1. The composite plate with delamination.

and 4 respectively. The mid-plane of each sub-laminate is defined by z_{ci} coordinate such that the displacements u_i, v_i and w_i $(i = 1, \ldots, 4)$ of an arbitrary point within each region, are expressed as follows

$$\begin{aligned} u_i &= u_{0i} + \Delta z_i \left[\varphi_i - \frac{\partial w_i}{\partial x} \right] - \frac{4\varphi_i}{3h_i^2} \Delta z_i^3 \\ v_i &= v_{0i} + \Delta z_i \left[\psi_i - \frac{\partial w_i}{\partial y} \right] - \frac{4\psi_i}{3h_i^2} \Delta z_i^3 \\ w_i &= w_{0i} \\ \Delta z_i &= z - z_{ci} \quad i = 1, \ldots, 4 \end{aligned} \tag{1}$$

In Eq. (1), the unknown rotations ϕ_i and ψ_i and the unknown mid-plane displacements u_{0i}, v_{0i}, and w_{0i}, are defined in each of the four regions, as time dependent functions of coordinates x and y. The sub-laminate thickness is denoted h_i $(i = 1\text{–}4)$. The above displacement field satisfies the stress free boundary conditions on both, the top and bottom surfaces of the plate and at the delamination interfaces. The Von-Karman strain–displacement relations are used for modeling moderate displacements and small rotations that characterize the deformed state. The total strain, ε_i, can be expressed in matrix form for each of the sub-laminates as follows

$$\begin{aligned} \boldsymbol{\varepsilon}_{i1} &= \begin{Bmatrix} \boldsymbol{\varepsilon}_{LNi} \\ \mathbf{0} \end{Bmatrix} + \Delta z_i \begin{Bmatrix} \boldsymbol{\varepsilon}_{1i} \\ \mathbf{0} \end{Bmatrix} + \Delta z_i^3 \begin{Bmatrix} \boldsymbol{\varepsilon}_{3i} \\ \mathbf{0} \end{Bmatrix} + \begin{Bmatrix} \mathbf{0} \\ \boldsymbol{\varepsilon}_{si} \end{Bmatrix} + \Delta z_i^2 \begin{Bmatrix} \mathbf{0} \\ \boldsymbol{\varepsilon}_{s2i} \end{Bmatrix} \\ \boldsymbol{\varepsilon}_{LNi} &= \boldsymbol{\varepsilon}_{0i} + \boldsymbol{\varepsilon}_{Ni} \end{aligned} \tag{2}$$

In Eq. (2), $\boldsymbol{\varepsilon}_{0i}$ and $\boldsymbol{\varepsilon}_{Ni}$ are the mid-plane and the nonlinear strains respectively. The quantities $\boldsymbol{\varepsilon}_{1i}$ and $\boldsymbol{\varepsilon}_{3i}$ are the bending strains corresponding to the linear and the cubic variations in z, $\boldsymbol{\varepsilon}_{si}$ is the mid-plane shear strain and $\boldsymbol{\varepsilon}_{s2i}$ is the shear strain corresponding to the quadratic variation in z.

The stress resultant vector is defined as

$$\hat{\boldsymbol{\sigma}}^{\mathrm{T}} = \left\{ \mathbf{N}^{\mathrm{T}} \mathbf{M}^{\mathrm{T}} \mathbf{P}^{\mathrm{T}} \mathbf{Q}^{\mathrm{T}} \mathbf{R}^{\mathrm{T}} \right\} \tag{3}$$

where $\mathbf{N}$, $\mathbf{M}$ and $\mathbf{Q}$ are the in-plane force resultant vectors and $\mathbf{P}$ and $\mathbf{R}$ denote the higher order stress resultants vectors. The constitutive relation can be written as

$$\hat{\boldsymbol{\sigma}} = \mathbf{C}\boldsymbol{\varepsilon} \tag{4}$$

where $\boldsymbol{\varepsilon}$ is the strain tensor and $\mathbf{C}$ is the stiffness matrix.

The equation of motion is derived using Hamilton's principle

$$\delta \Pi = \int_{t_1}^{t_2} (\delta T - \delta U + \delta W)\, \mathrm{d}t = 0 \tag{5}$$

where T, U and W are the kinetic energy, the strain energy and the work done by the buckling load respectively.

3. Finite element formulation

The governing equation of the composite plate, is obtained using Hamilton's principle (Eq. (5)). The finite element analysis is performed using a quadrilateral element with four nodes and eight degrees of freedom per node. In matrix form, the governing equation of the plate is obtained as follows

$$\mathbf{M}\ddot{\mathbf{q}} + \mathbf{K}_{\mathrm{L}}\mathbf{q} + F_x \mathbf{K}_{\mathrm{G}}\mathbf{q} = 0 \tag{6}$$

where $\mathbf{M}$ is the mass matrix, $\mathbf{K}_{\mathrm{L}}$ is the linear stiffness matrix, $\mathbf{K}_{\mathrm{G}}$ is the geometric stiffness matrix and $\mathbf{q}$ is the vector of nodal unknowns. The nonlinear matrices obtained from the corresponding terms in the Von-Karman strain–displacement relations have been ignored in the present study.

In modeling delamination, continuity conditions are imposed at the nodal unknowns $(u, \varphi, v, \psi, w, \partial w/\partial x, \partial w/\partial y, \partial^2 w/\partial x\,\partial y)$ of the upper and lower sub-laminates and the nodal unknowns of the left and right sub-laminates after assembling the global matrices. For example the continuity conditions between the left (index "3") and upper (index "1") sub-laminates (Fig. 1) are written as

$$\begin{aligned}
&u_{03} + \left[z_{c1} - \frac{4}{3h_3^2} z_{c1}^3\right]\alpha_3 - z_{c1}\frac{\partial w_{03}}{\partial x} - u_{01} = 0\\
&\left[\frac{\partial u_3}{\partial z}\right]_{z=z_{c1}} - \left[\frac{\partial u_1}{\partial z}\right]_{z=0} = 0\\
&v_{03} + \left[z_{c1} - \frac{4}{3h_3^2} z_{c1}^3\right]\beta_3 - z_{c1}\frac{\partial w_{03}}{\partial y} - v_{01} = 0\\
&\left[\frac{\partial v_3}{\partial z}\right]_{z=z_{c1}} - \left[\frac{\partial v_1}{\partial z}\right]_{z=0} = 0
\end{aligned} \tag{7a}$$

$$\begin{aligned}
w_{03} - w_{01} &= 0\\
\frac{\partial w_{03}}{\partial x} - \frac{\partial w_{01}}{\partial x} &= 0\\
\frac{\partial w_{03}}{\partial y} - \frac{\partial w_{01}}{\partial y} &= 0\\
\frac{\partial^2 w_{03}}{\partial x\,\partial y} - \frac{\partial^2 w_{01}}{\partial x\,\partial y} &= 0
\end{aligned} \tag{7b}$$

The constraint conditions (Eqs. (7a) and (7b)) can be written in matrix form for the entire plate as follows

$$\mathbf{C}_q\mathbf{q} = \mathbf{0} \tag{8}$$

where $\mathbf{C}_q$ represents the constraint equations matrix and $\mathbf{q}$ represents the unknown vector. To apply the transformation matrix method (Cook et al., 1989), the unknown vector is partitioned as follows

$$\mathbf{q} = \begin{Bmatrix} \mathbf{q}_r \\ \mathbf{q}_c \end{Bmatrix} \tag{9}$$

where $\mathbf{q}_r$ represents the vector of the independent degrees of freedom, to be retained, and $\mathbf{q}_c$ represents the vector of the dependent degrees of freedom, to be condensed out. The same partition operation is applied to the assembled stiffness, mass and geometric matrix as well as to the constraint matrix which is written as

$$[\,\mathbf{C}_r \quad \mathbf{C}_c\,]\begin{Bmatrix} \mathbf{q}_r \\ \mathbf{q}_c \end{Bmatrix} = \mathbf{0} \tag{10}$$

Further, the unknown vector can be expressed in terms of the vector of the independent degrees of freedom as follows

$$\mathbf{q} = \mathbf{T}\mathbf{q}_r \tag{11}$$

where $\mathbf{T}$ represents the transformation matrix

$$\mathbf{T} = \begin{bmatrix} \mathbf{I} \\ -\mathbf{C}_c^{-1}\mathbf{C}_r \end{bmatrix} \tag{12}$$

The governing equation of the plate can now be written in terms of the vector of independent degrees of freedom as follows

$$\mathbf{M}_d\ddot{\mathbf{q}}_r + \mathbf{K}_d\mathbf{q}_r + F_x\mathbf{K}_{\mathrm{G}d}\mathbf{q}_r = 0 \tag{13}$$

where the new mass ($\mathbf{M}_d$), stiffness ($\mathbf{K}_d$) and geometric ($\mathbf{K}_{\mathrm{G}d}$) matrices are obtained from the assembled mass, stiffness and geometric matrices through the following matrix operations

$$\begin{aligned} \mathbf{K}_d &= \mathbf{T}^{\mathrm{T}}\mathbf{K}\mathbf{T} \\ \mathbf{M}_d &= \mathbf{T}^{\mathrm{T}}\mathbf{M}\mathbf{T} \\ \mathbf{K}_{\mathrm{G}d} &= \mathbf{T}^{\mathrm{T}}\mathbf{K}_{\mathrm{G}}\mathbf{T} \end{aligned} \tag{14}$$

4. Stability analysis

The stability analysis of the plate is performed by expressing the dynamic buckling load, F_x, in terms of a static and a dynamic component, both of them written in terms of the critical buckling load, P_{cr}, as follows

$$F_x = \alpha_0 P_{\mathrm{cr}} + \alpha_1 P_{\mathrm{cr}} \cos(\theta t) \tag{15}$$

where α_0 and α_1 are the static and dynamic parameters taking values from 0 to 1. Substituting for the buckling load (Eq. (15)) in Eq. (6) or in Eq. (13), the governing equation of the plate is written as follows

$$\mathbf{M}\ddot{\mathbf{q}} + [\mathbf{K} + \alpha_0 P_{\mathrm{cr}}\mathbf{K}_{\mathrm{G}}]\mathbf{q} + (\alpha_1 P_{\mathrm{cr}} \cos(\theta t))\mathbf{K}_{\mathrm{G}}\mathbf{q} = \mathbf{0} \tag{16}$$

Note that in the above equation, the generic matrices $\mathbf{M}$, $\mathbf{K}$ and $\mathbf{K}_{\mathrm{G}}$ are the mass, the stiffness and the geometric matrices for the plate with or without delamination and $\mathbf{q}$ is the generic unknown vector.

Eq. (16) is a Mathieu type equation, describing the nonlinear instability behavior of the plate subjected to a periodic in-plane compressive load. The generalized eigenvalue problem obtained from Eq. (16) by neglecting both terms containing P_{cr} is solved to obtain the natural frequencies of the plate (Eq. (17)).

$$\mathbf{M}\ddot{\mathbf{q}} + \mathbf{K}\mathbf{q} = \mathbf{0} \tag{17}$$

If the harmonic and the mass terms are neglected in Eq. (16), the new generalized eigenvalue problem (Eq. (18)) yields the critical buckling load.

$$[\mathbf{K} + \lambda_{\mathrm{cr}}\mathbf{K}_{\mathrm{G}}]\mathbf{q} = \mathbf{0} \tag{18}$$

If only the harmonic term is ignored in Eq. (16), the natural frequency of the loaded plate is obtained (Eq. (19)).

$$\mathbf{M}\ddot{\mathbf{q}} + [\mathbf{K} + \alpha_0 P_{\mathrm{cr}}\mathbf{K}_{\mathrm{G}}]\mathbf{q} = \mathbf{0} \tag{19}$$

The instability regions are determined by the boundaries of instability (Bolotin, 1964), which represent the periodic solutions of Eq. (16). These solutions are as follows

$$\begin{aligned}\mathbf{q} &= \mathbf{b}_0 + \sum_{i=2,4,\ldots}^{\infty} (\mathbf{a}_i \sin(\mathrm{i}\theta t/2) + \mathbf{b}_i \cos(\mathrm{i}\theta t/2)) \\ \mathbf{q} &= \sum_{i=1,3,\ldots}^{\infty} (\mathbf{a}_i \sin(\mathrm{i}\theta t/2) + \mathbf{b}_i \cos(\mathrm{i}\theta t/2))\end{aligned} \tag{20}$$

where $\mathbf{a}_i$ and $\mathbf{b}_i$ are unknown coefficient vectors and θ represents the frequency.

Substituting the solutions (Eq. (20)) into Eq. (16) and by grouping the sine and cosine terms, two sets of linear algebraic equations in $\mathbf{a}_i$ and $\mathbf{b}_i$ are obtained for each solution. To obtain nontrivial coefficient vectors $\mathbf{a}_i$ and $\mathbf{b}_i$, the determinant of the coefficient matrix must be zero for each of the four sets. These determinants are infinite since the series in Eq. (20) are infinite, and they belong to a class of converging determinants called normal determinants (Bolotin, 1964). Considering only the first terms in the series (Eq. (20)), the solution is approximated by

$$\begin{aligned}\mathbf{q} &= \mathbf{b}_0 + \mathbf{a}_2 \sin\theta t + \mathbf{b}_2 \cos\theta t \\ \mathbf{q} &= \mathbf{a}_1 \sin\frac{\theta t}{2} + \mathbf{b}_1 \cos\frac{\theta t}{2}\end{aligned} \tag{21}$$

By substituting the one-term series solutions (Eq. (21)) into the Mathieu equation (16) the following eigenvalue problems are obtained

$$\begin{aligned}&\mathbf{K} + (\alpha_0 \pm 0.5\alpha_1)\lambda_{\mathrm{cr}}\mathbf{K}_{\mathrm{G}} - 0.25\mathbf{M}\theta_1^2 = \mathbf{0} \\ &\mathbf{K} + \alpha_0\lambda_{\mathrm{cr}}\mathbf{K}_{\mathrm{G}} - \mathbf{M}\theta_1^2 = \mathbf{0} \\ &\begin{bmatrix} \mathbf{K} + \alpha_0\lambda_{\mathrm{cr}}\mathbf{K}_{\mathrm{G}} & 0.5\alpha_1\lambda_{\mathrm{cr}}\mathbf{K}_{\mathrm{G}} \\ \alpha_1\lambda_{\mathrm{cr}}\mathbf{K}_{\mathrm{G}} & \mathbf{K} + \alpha_0\lambda_{\mathrm{cr}}\mathbf{K}_{\mathrm{G}} \end{bmatrix} - \begin{bmatrix} \mathbf{0} & \mathbf{0} \\ \mathbf{0} & \mathbf{M} \end{bmatrix}\theta_1^2 = \mathbf{0}\end{aligned} \tag{22}$$

where θ_1 represents the first order approximation of the parametric resonance frequency (Bolotin, 1964).

The two-terms solutions obtained from Eq. (20) are

$$\begin{aligned}\mathbf{q} &= \mathbf{b}_0 + \mathbf{a}_2 \sin\theta t + \mathbf{b}_2 \cos\theta t + \mathbf{a}_4 \sin 2\theta t + \mathbf{b}_4 \cos 2\theta t \\ \mathbf{q} &= \mathbf{a}_1 \sin\frac{\theta t}{2} + \mathbf{b}_1 \cos\frac{\theta t}{2} + \mathbf{a}_3 \sin\frac{3\theta t}{2} + \mathbf{b}_3 \cos\frac{3\theta t}{2}\end{aligned} \tag{23}$$

For nontrivial solutions, the resulting determinants must be zero. This leads to the generalized eigenvalue problems which solved in an iterative manner results in the second approximation of first two instability regions. For example, the iterative form of the first two generalized eigenvalue problems takes the form

$$\begin{bmatrix} \mathbf{K}^* \pm 0.5\alpha_1\lambda_{\mathrm{cr}}\mathbf{K}_{\mathrm{G}} & 0.5\alpha_1\lambda_{\mathrm{cr}}\mathbf{K}_{\mathrm{G}} \\ 0.5\alpha_1\lambda_{\mathrm{cr}}\mathbf{K}_{\mathrm{G}} & \mathbf{K}^* - 2.25\mathbf{M}\theta_1^2 \end{bmatrix} - \begin{bmatrix} 0.25\mathbf{M} & \mathbf{0} \\ \mathbf{0} & \mathbf{0} \end{bmatrix}\theta_2^2 = \mathbf{0} \tag{24}$$

$$\begin{bmatrix} \mathbf{K}^* & 0.5\alpha_1\lambda_{\mathrm{cr}}\mathbf{K}_{\mathrm{G}} & \mathbf{0} \\ 0.5\alpha_1\lambda_{\mathrm{cr}}\mathbf{K}_{\mathrm{G}} & \mathbf{K}^* - 4\mathbf{M}\theta_1^2 & 0.5\alpha_1\lambda_{\mathrm{cr}}\mathbf{K}_{\mathrm{G}} \\ \mathbf{0} & 0.5\alpha_1\lambda_{\mathrm{cr}}\mathbf{K}_{\mathrm{G}} & \mathbf{K}^* - 9\mathbf{M}\theta_1^2 \end{bmatrix} - \begin{bmatrix} \mathbf{M} & \mathbf{0} & \mathbf{0} \\ \mathbf{0} & \mathbf{0} & \mathbf{0} \\ \mathbf{0} & \mathbf{0} & \mathbf{0} \end{bmatrix}\theta_2^2 = \mathbf{0} \tag{25a}$$

$$\begin{bmatrix} \mathbf{K}^* & 0.5\alpha_1\lambda_{\mathrm{cr}}\mathbf{K}_{\mathrm{G}} & \mathbf{0} & \mathbf{0} \\ \alpha_1\lambda_{\mathrm{cr}}\mathbf{K}_{\mathrm{G}} & \mathbf{K}^* & 0.5\alpha_1\lambda_{\mathrm{cr}}\mathbf{K}_{\mathrm{G}} & \mathbf{0} \\ \mathbf{0} & 0.5\alpha_1\lambda_{\mathrm{cr}}\mathbf{K}_{\mathrm{G}} & \mathbf{K}^* - 4\mathbf{M}\theta_1^2 & 0.5\alpha_1\lambda_{\mathrm{cr}}\mathbf{K}_{\mathrm{G}} \\ \mathbf{0} & \mathbf{0} & 0.5\alpha_1\lambda_{\mathrm{cr}}\mathbf{K}_{\mathrm{G}} & \mathbf{K}^* - 9\mathbf{M}\theta_1^2 \end{bmatrix} - \begin{bmatrix} \mathbf{0} & \mathbf{0} & \mathbf{0} & \mathbf{0} \\ \mathbf{0} & \mathbf{M} & \mathbf{0} & \mathbf{0} \\ \mathbf{0} & \mathbf{0} & \mathbf{0} & \mathbf{0} \\ \mathbf{0} & \mathbf{0} & \mathbf{0} & \mathbf{0} \end{bmatrix}\theta_2^2 = \mathbf{0} \tag{25b}$$

where the following notation has been used

$$\mathbf{K}^* = \mathbf{K} + \alpha_0 \lambda_{cr} \mathbf{K}_G \tag{26}$$

The $\pm$ sign in Eq. (24) differentiates the upper and lower boundaries of the first instability region. The upper and lower boundaries of the second instability region result from Eqs. (25a) and (25b) respectively. In Eqs. (24), (25a) and (25b), θ_1 and θ_2 represent the first and the second order approximation of the parametric resonance frequency.

5. Numerical considerations

The free vibration, buckling and stability eigenvalue problems derived from Eq. (16) are solved using LAPAC sub-routines within an in-house developed FORTRAN code. When compared to the matrix size involved in the vibration (Eqs. (17) and (19)) and buckling (Eq. (18)) equations, the matrices involved in the dynamic stability eigenvalue problem of Eq. (24) are four times larger while the matrices in Eqs. (25a) and (25b) are nine and sixteen times larger, respectively. To reduce the size of the stability eigenvalue problems to the size of the free vibration problem, a condensation procedure has been performed for Eqs. (24), (25a) and (25b). The obtained condensed form of these equations is

$$[\mathbf{K}^* \pm 0.5\alpha_1 \lambda_{cr} \mathbf{K}_\sigma - 0.25\alpha_1^2 \lambda_{cr}^2 \mathbf{K}_\sigma \mathbf{K}^* - 2.25\mathbf{M}\theta_1^2]^{-1} \mathbf{K}_\sigma - 0.25\mathbf{M}\theta_2^2 = 0 \tag{27}$$

$$\left[\mathbf{K}^* - 0.25\alpha_1^2 \lambda_{cr}^2 \mathbf{K}_\sigma \mathbf{K}_T \mathbf{K}_\sigma\right] - \mathbf{M}\theta_2^2 = 0 \tag{28a}$$

$$\left[\mathbf{K}^* - 0.5\alpha_1^2 \lambda_{cr}^2 \mathbf{K}_\sigma [\mathbf{K}^*]^{-1} \mathbf{K}_\sigma - 0.25\alpha_1^2 \lambda_{cr}^2 \mathbf{K}_\sigma \mathbf{K}_T \mathbf{K}_\sigma\right] - \mathbf{M}\theta_2^2 = 0 \tag{28b}$$

where in addition to the notation defined by Eq. (26), the following notation has been used

$$\mathbf{K}_T = \left[\mathbf{K}^* - 4\mathbf{M}\theta_1^2 - 0.25\alpha_1^2 \lambda_{cr}^2 \left[\mathbf{K}^* - 9\mathbf{M}\theta_1^2\right]^{-1} \mathbf{K}_\sigma\right]^{-1} \tag{29}$$

6. Numerical results

Numerical validation of the governing equation of the composite plate undergoing combined static and dynamic buckling (Eq. (16)) is performed by solving the corresponding free vibration (Eq. (17)) and buckling (Eq. (18)) eigenvalue problems. The natural frequency results are compared with available experimental data (Shen and Grady, 1992) and with NASTRAN 3D solutions for plates with and without delaminations. The critical buckling load results are compared with those obtained using classical and FSDTs and also referred to experimental results. The delamination modeling capability of the developed finite element model is tested through parametric studies involving horizontal and vertical delamination placement. Finally, the parametric resonance phenomenon is investigated for various loading conditions and the delamination effect on the instability regions is presented. The effect of ply arrangement is also investigated.

Numerical results are presented for graphite/epoxy rectangular plates of varying stacking sequence, delamination lengths and boundary conditions. The laminates are made out of eight identical plies with material properties: $E_1 = 1.344 \times 10^5$ MPa, $E_2 = E_3 = 1.034 \times 10^4$ MPa, $G_{12} = G_{13} = 4.999 \times 10^3$ MPa, $G_{23} = 1.999 \times 10^3$ MPa; $v_{12} = v_{13} = v_{23} = 0.33$. The plate has length $L = 127$ mm and width $b = 12.7$ mm. Three different plate thicknesses, $h = 1.016$ mm, $h = 5.08$ mm, and $h = 10.16$ mm resulting in three cases,

Table 1
CLPT, FSDT and HOT vs. NASTRAN 3D and experimental results

Case	L/h		CLPT	FSDT	Exp. [14] Shen and Grady (1992)	NASTRAN 3D	HOT
1	125	ω_1 (Hz)	82.15	82.12	79.83	81.98	82.12
		P_{cr} (N)	16.43	16.38			16.33
2		ω_1 (Hz)	522.85	521.15			520.72
		P_{cr} (N)	261.62	260.11			259.73
1	12.5	ω_1 (Hz)	820.52	795.09			789.22
		P_{cr} (N)	16 344	15 772			15 364
2		ω_1 (Hz)	4664.4	4058.6			3885.5
		P_{cr} (N)	261 623	165 644			152 179

$L/h = 125$, $L/h = 25$, and $L/h = 12.5$, are analyzed. The finite element analysis is performed using 10 quadrilateral elements along the length of the plate with four nodes and eight degrees of freedom per node.

First, validation of the theory is performed by analyzing composite plates without delamination. In this study two types of boundary conditions are studied. Case 1: one of the short edges fixed and the opposite edge loaded with dynamic buckling force and case 2: both short edges fixed and dynamic buckling load applied on one of them; the long edges are free in both cases. The first natural frequency and the critical buckling load are computed for each combination of boundary conditions and thickness using CLPT, FSDT and HOT. The obtained results are compared with experimental results of Shen and Grady (1992) for the thin plate ($L/h = 125$) and case 1 type boundary conditions. The results are also validated by comparison with 3D NASTRAN solutions obtained using 10 CHEXA elements along the length of the

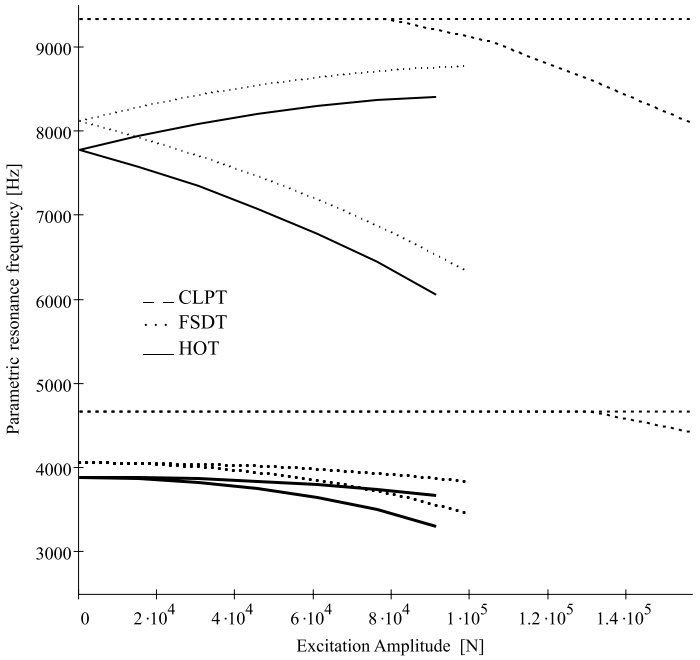

Fig. 2. The second order approximation of the instability regions for the three plate theories, $L/h = 12.5$, case 2.

Table 2
First two bending natural frequencies vs. experimental results; buckling load

Delamination length (mm)	Exp. [13]	NASTRAN 3D		HOT			
	ω_1 (Hz)	ω_1 (Hz)	ω_2 (Hz)	ω_1 (Hz)	ω_2 (Hz)	P_{cr} (N)	P_{cr} (%)
0	79.83	81.75	510.70	82.12	513.30	16.336	100.00
25.4	78.17	80.43	504.18	81.19	509.24	16.068	98.36
50.8	75.38	75.14	478.66	76.48	469.02	15.054	92.15
76.2	66.96	66.53	399.36	67.26	369.08	12.712	77.82
101.6	57.54	55.81	305.75	56.64	325.79	9.934	60.81

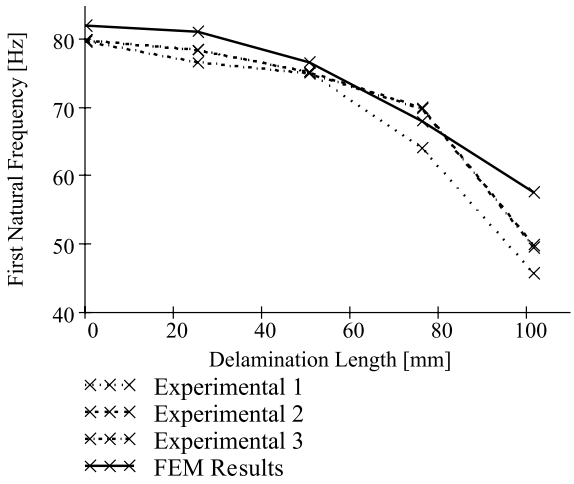

Fig. 3. The natural frequency of the loaded plate vs. experimental results [13] for $L/h = 125$ and various delamination lengths placed in vertical position 1.

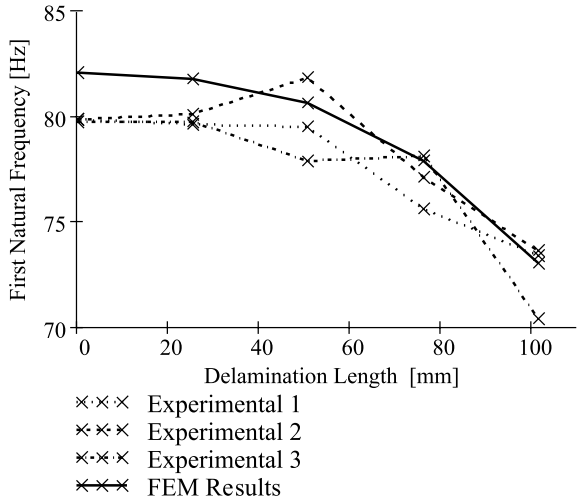

Fig. 4. The natural frequency of the loaded plate vs. experimental results [13] for $L/h = 125$ and various delamination lengths placed in vertical position 3.

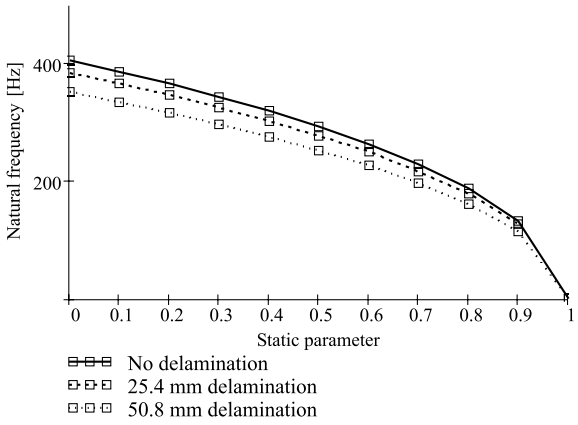

Fig. 5. The natural frequency of the loaded plate $L/h = 25$.

plate, each lamina being modeled by a single layer of elements. These results, summarized in Table 1, indicate that the CLPT and the FSDT slightly over predict the natural frequency while HOT results are closer to the experimental values and to the NASTRAN results. For both types of boundary conditions, the CLPT and the FSDT over predict the natural frequencies and the critical buckling load compared to the HOT. These deviations are more significant for thicker plates ($L/h = 12.5$). This is due to the fact that the HOT is more accurate in modeling the transverse shear effects. These effects increase with plate thickness.

The stability regions obtained using the three plate theories are presented in Fig. 2. It can be observed that the parametric resonance frequencies obtained using CLPT and FSDT for the thick composite plate

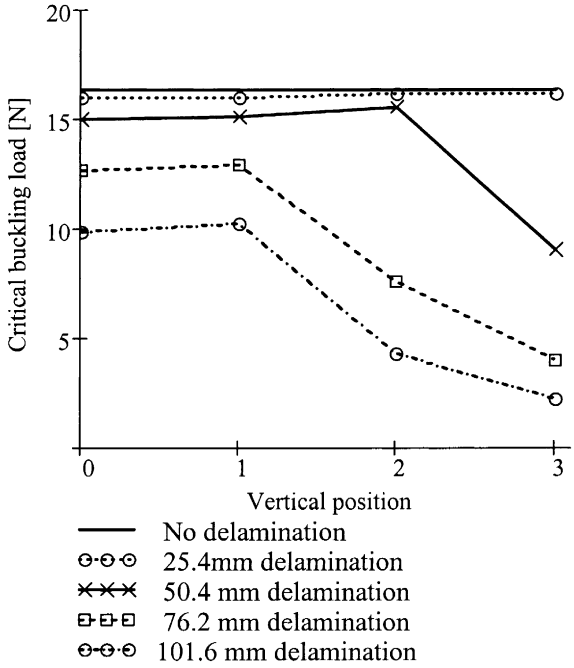

Fig. 6. Critical buckling load vs. vertical position for various delamination lengths.

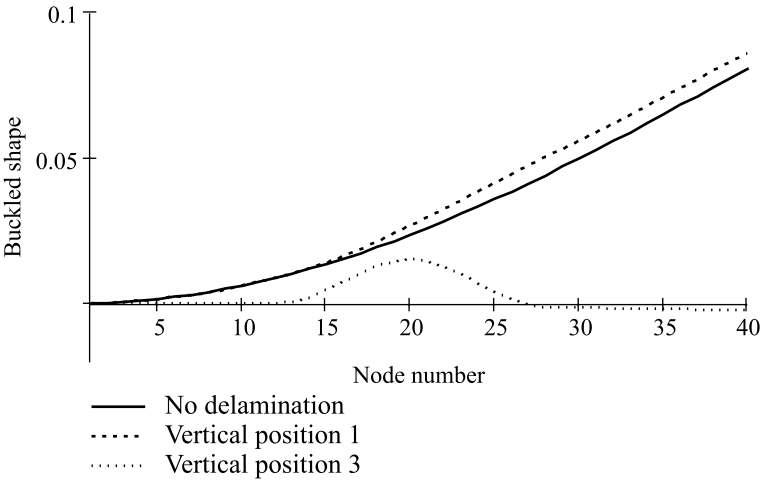

Fig. 7. The buckled shape of the plate for a 50.8 mm delamination and vertical position 0, 1 and 3.

$(L/h = 12.5)$ in case 2 are higher than those obtained using HOT. Due to the presence of significant transverse shear stress in thick composites, maximum deviations are observed from CLPT, which completely ignores shear effects. Noticeable deviations in the instability regions are observed from FSDT as well.

Next, the case of a composite plate with delamination is considered. The natural frequencies of the plate with delamination are compared for validation purposes with available experimental data (Shen and Grady, 1992) and with 3D NASTRAN solutions for a cantilever composite plate (case 1) using $40 \times 5 \times 8$

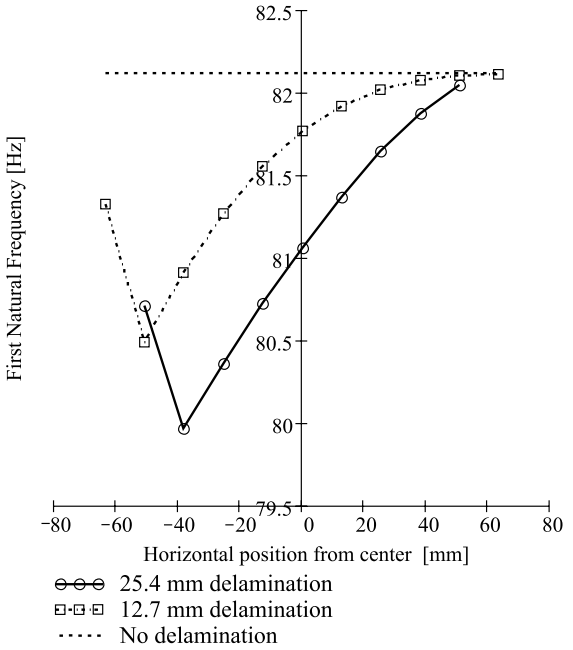

Fig. 8. The natural frequency of the plate vs. the horizontal position of 12.7 and 25.4 mm mid-plane delaminations, $L/h = 125$.

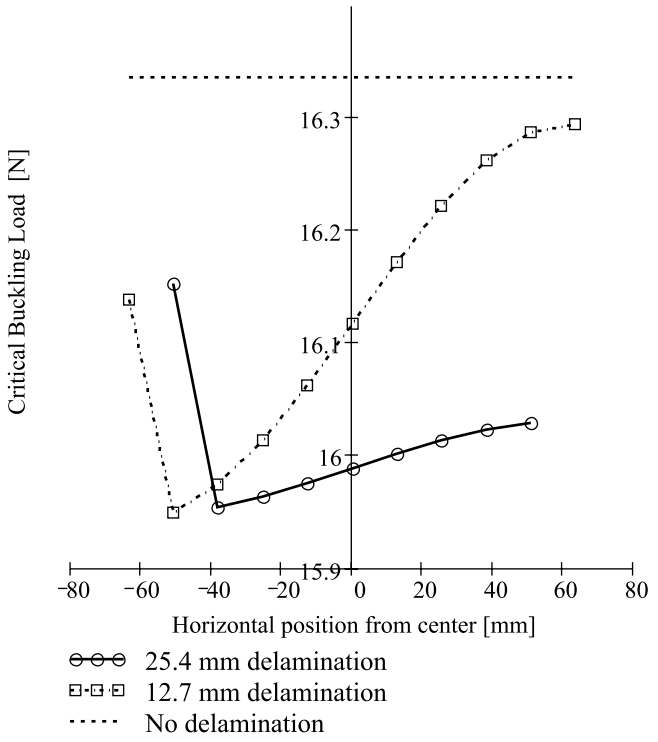

Fig. 9. The critical buckling load of the plate vs. the horizontal position of 12.7 and 25.4 mm mid-plane delaminations $L/h = 125$.

CHEXA elements. The material properties and the dimensions of the plate are the same as those used for the composite plate without delamination. Four mid-plane delamination lengths are considered representing 20%, 40%, 60% and 80% of the total plate length. The delamination is placed at equal distance from the ends of the plate. The plate is meshed using a single row of 40 plate elements along the length, the lower sub-laminate being added during the assembling procedure and constrained using the procedure described by Eqs. (7a)–(14). For the NASTRAN analysis, the delamination is modeled by creating new nodes in the mid-plane of the plate without delamination and by modifying the connectivity of lower sub-laminate elements at the delamination free surface. Table 2 presents comparison of the first two bending natural frequencies obtained using the HOT based finite element model, the experimental results obtained by Shen and Grady (1992) as well as the results of the 3D NASTRAN analysis. As shown, the HOT results agree very well with the experimental results. Excellent correlation is also observed with the results of the 3D NASTRAN analysis, which is computationally expensive. Similar observations are made for the torsional and the lateral bending modes. The decrease in natural frequencies is due to the decrease in the plate stiffness caused by delamination. Similar results were reported by Campanelli and Engblom (1995).

The effect of delamination length on the critical buckling load of the plate has also been investigated for validation purposes. The results are presented in Table 2 and show decrease in the load capacity of the plate. This is once again due to the reduction in plate stiffness caused by the delamination.

Another validation of the HOT based finite element procedure is presented in Figs. 3 and 4 where the natural frequencies are compared with three sets of experimental data of Shen and Grady (1992). These results are presented for delaminations of various lengths placed in the vertical locations 1 and 3 respectively (Fig. 1).

For the plate statically loaded with $\alpha_0 P_{cr}$, (Eq. (19)) the variations in the first natural frequency of the loaded plate with respect to the static parameter (α_0) are presented in Fig. 5 for $L/h = 25$ and three different delamination lengths. It can be observed that delamination decrease the natural frequency of the loaded plate. For the static load corresponding to the critical buckling load, the frequency is zero since the plate has already buckled and has changed its equilibrium state.

The effect of the through-the-thickness vertical location of delamination on the critical buckling load of the plate is presented in Fig. 6. The figure shows that large delaminations that are closer to the free surface reduce the critical buckling more than those placed closer to the mid-plane. This is due to the fact that the thinner sub-laminate above the delamination undergoes local buckling under a much smaller force compared to a thicker sub-laminate. The resulting ply arrangements in the two sub-laminates also influence the value of the critical buckling load through inherent coupling effects. For example, the cases with small delaminations, 25.4 and 50.8 mm, which do not exhibit local buckling, exhibit a small increase in the critical buckling load when placed in vertical locations 1 and 2 compared to the mid-plane placement. The buckled shape of the plate is presented in Fig. 7 for a 50.8 mm delamination placed at vertical locations 1 and 3 and for a plate without delamination. Once again, local buckling is observed when the delamination is placed closer to the free surface of the plate (vertical location 3) while for the delamination placed closer to the mid-plane, the buckled shape conserves its global characteristics with small deviations from the shape of the plate without delamination.

For mid-plane delaminations, a parametric study is performed to investigate the effect of delamination placement along the length on the natural frequencies and critical buckling loads of the plate. The results are presented in Figs. 8–10. The large negative values on the x-axis correspond to the delamination placed in close vicinity of the fixed end while the large positive values on the x-axis correspond to free edge delamination. As shown in Fig. 8, the first natural frequency of the plate with delamination varies from

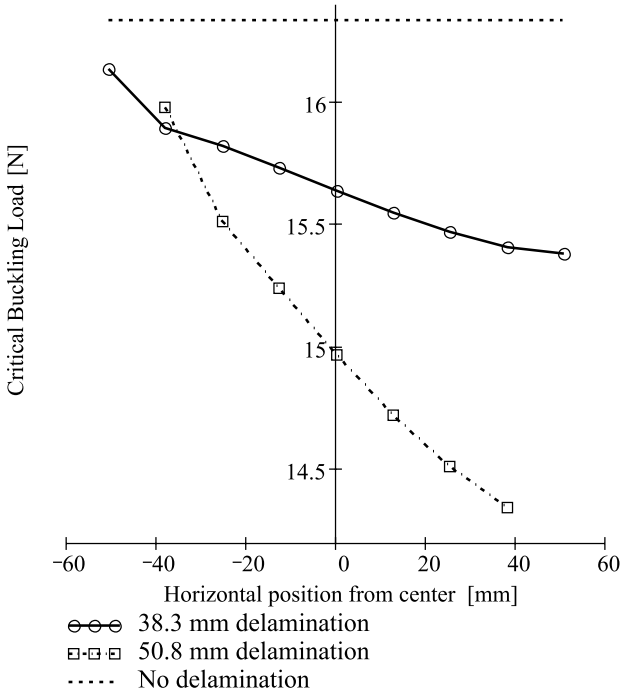

Fig. 10. The critical buckling load of the plate vs. the horizontal position of 38.3 and 50.8 mm mid-plane delaminations $L/h = 125$.

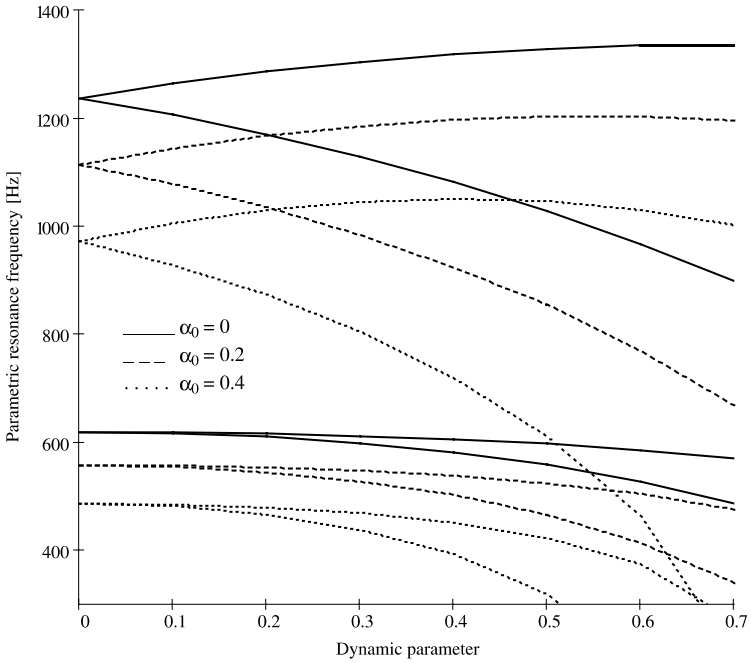

Fig. 11. The influence of the static component of the buckling force on the instability regions, $L/h = 12.5$, 50.8 mm delamination.

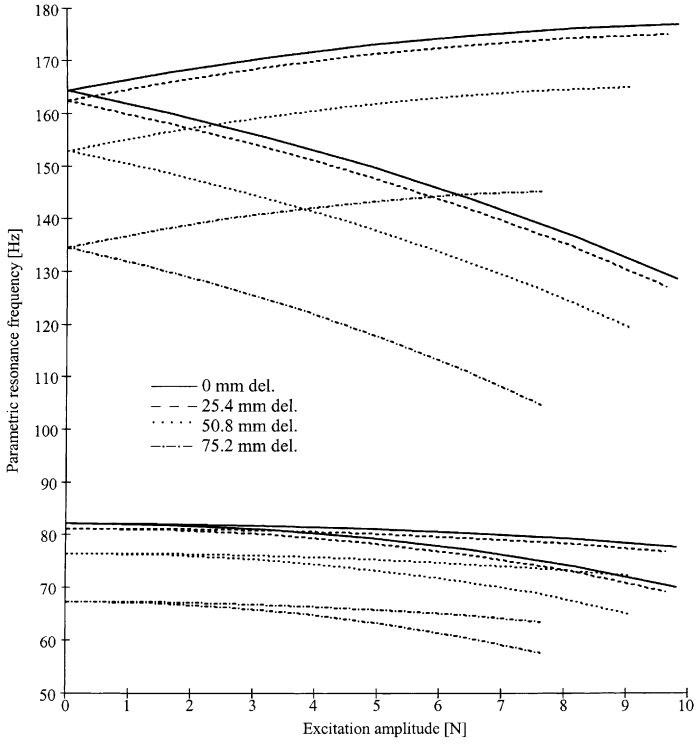

Fig. 12. The influence of the delamination length on the instability regions, $L/h = 125$.

values close to those obtained for the plate without delamination to much lower values as the delamination placement approaches the fixed end of the plate. A slight increase in natural frequency is observed for the limiting case when delamination is initiated at the fixed end of the plate. The same behavior is observed with the critical buckling load of the plate for small delaminations (Fig. 9). However with large delaminations which trigger local buckling phenomenon, the slope of the curves is reversed as seen in Fig. 10.

Next investigation is performed on the plate stability characteristics. As observed by Bolotin (1964), the first parametric resonance frequency of the first instability region is found to be double the value of the first natural frequency and the first parametric resonance frequency of the second instability region equals the first natural frequency. First, the effect of the static component, whose magnitude is governed by the static parameter (α_0), on the instability regions, is studied. The results are presented in Fig. 11 for the thick composite plate ($L/h = 12.5$) with a 40% delamination and show that the width of the instability regions increases with increase in static force. Also the instability regions are shifted to lower parametric resonance frequency values which correspond to double the value of natural frequency of the statically loaded plate (Eq. (19)).

Next, the influence of the delamination length on the instability regions is examined and the results are presented in Fig. 12 for the thin composite plate ($L/h = 125$). As the delamination length increases, the parametric resonance frequencies decrease and therefore the instability regions are shifted to lower frequencies. The first parametric resonance frequency is equal to double the value of the natural frequency of the plate. The decrease in critical buckling load caused by increased delamination length is reflected trough a reduction in the amplitude of excitation.

Finally, a parametric study is performed to investigate the effect of ply orientation on the instability regions. The results obtained for a crossply $[(0/90)_2]_s$ and an angle ply arrangement $[(-45/45)_2]_s$ with the same length to thickness ratio ($L/h = 25$) are presented in Fig. 13 for a 20% delamination. The ply

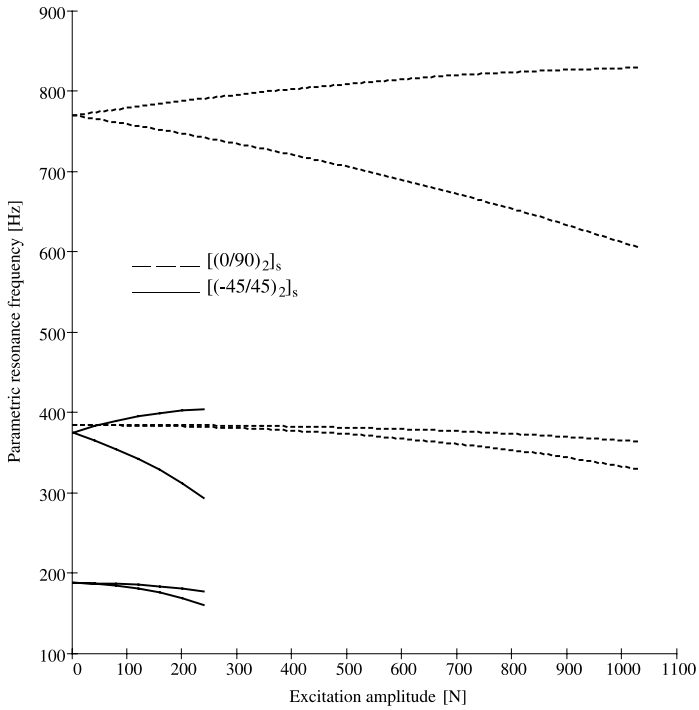

Fig. 13. The influence of the ply orientation on the instability regions, $L/h = 25$.

orientation can substantially change the stability regions first by changing the placement of the instability regions as a result of change in parametric resonance frequency and second by affecting the width and the extension of the instability region through changes in critical buckling load.

7. Concluding remarks

A higher order plate theory based finite element model has been developed for studying the parametric resonance of composite plates with and without delaminations. The theory assumes through the thickness cubic variations for in-plane displacements and satisfies the stress free boundary conditions. Numerical results are presented for $[(0/90)_2]_s$ graphite/epoxy composite cantilever plate with a symmetric through the width delamination. Comparisons with the classical and the first order shear deformation plate theories are presented for the plate without delamination under symmetric and nonsymmetric boundary conditions. The natural frequencies, the critical buckling load and the instability regions are investigated for various plate thickness and varying delamination size and locations. The influence of the ply orientation on the instability region is also investigated. The following observations are made from this study:

1. The bending natural frequencies and the critical buckling loads of composite plates with and without delamination, are in good correlation with available experimental data and with 3D NASTRAN results.
2. In case of plates without delamination, both the classical and the first order theories over predict the natural frequencies and the critical buckling load for both types of boundary conditions studied. The deviations increase with plate thickness due to increased transverse shear effects. The instability regions differ dramatically, especially for thicker plates.
3. The natural frequencies and the critical buckling load decrease with increase in delamination length. This is due to the reduction in stiffness caused by delamination.
4. The placement of the delamination, both through-the-thickness and along the length, affects the natural frequencies and the critical buckling load through specific local buckling phenomena and sub-laminate coupling effects.
5. The width of the instability regions increases with increase in both, static and dynamic loads.
6. Delamination affects the instability regions by shifting them to lower parametric resonance frequencies and by modifying their extension.
7. Ply orientations substantially change the placement and size of the instability regions.

Acknowledgements

The support of the present research by US Army Research Office, grant #DAAH04-94-G-0157, Technical Monitor, Dr. Gary Anderson is acknowledged.

References

Balamurugan, M., Ganapathi, M., Varadan, T.K., 1996. Nonlinear dynamic instability of laminated composite plates using finite element method. Computers and Structures 60 (1), 125–130.

Bert, C.W., Birman, V., 1987. Dynamic instability of shear deformable antisymmetric angle-ply plates. International Journal of Solids and Structures 23 (7), 1053–1061.

Bolotin, V.V., 1964. The Dynamic Stability of Elastic Systems. Holen-Day, San Francisco.

Campanelli, R.W., Engblom, J.J., 1995. The effect of delaminations in graphite/PEEK composite plates on modal dynamic characteristics. Composite Structures 31 (1), 195–202.

Chattopadhyay, A., Gu, H., 1994. New higher order plate theory in modeling delamination buckling of composite laminates. AIAA Journal 32 (8), 1709–1716.

Chattopadhyay, A., Radu, A.G., 2000. Dynamic instability of composite laminates using a higher order theory. Computers and Structures 77 (5), 453–460.

Cook, R.D., Malkus, D.S., Plesha, M.E., 1989. Concepts and Applications of Finite Element Analysis. Wiley, New York.

Gu, H., Chattopadhyay, A., 1996. Delamination buckling and postbuckling of composite cylindrical shells. AIAA Journal 34 (6), 1279–1286.

Gu, H., Chattopadhyay, A., 1998. Elasticity approach for delamination buckling of composite beam plates. Composite Structures 36 (8), 1529–1534.

Karadomateas, G.A., Schmueser, D.W., 1988. Buckling and postbuckling of delaminated composites under compressive loads including transverse shear effects. AIAA Journal 26 (3), 337–342.

Reddy, J.N., 1984. A simple higher-order theory for laminated composite plates. Journal of Applied Mechanics 51 (12), 745–752.

Reddy, J.N., Phan, N.D., 1985. Stability and vibration of isotropic, orthotropic and laminated plates according to a higher order shear deformation theory. Journal of Sound and Vibration 98 (2), 157–170.

Schivakumar, K.N., Whitcomb, J.D., 1985. Buckling of a sublaminate in a quasi-isotropic composite laminate. Journal of Composite Materials 19 (1), 2–18.

Shen, M.H.H., Grady, J.E., 1992. Free vibrations of delaminated beams. AIAA Journal 60 (5), 1361–1370.

Simitses, G.J., Sallam, S., Yin, W.L., 1985. Effect of delamination of axially loaded homogenous laminated plate. AIAA Journal 23 (9), 1437–1444.

Srinivasan, R.S., Chelepandi, P., 1986. Dynamic stability of rectangular laminated composite plate. Computers and Structures 24 (2), 233–238.